Aalborg Universitet

A Two-layer Distributed Cooperative Control Method for Islanded Networked Microgrid Systems

Wu, Xiaoyu; Xu, Yin; Wu, Xiangyu; He, Jinghan; Guerrero, Josep M.; Liu, Chen-Ching; Schneider, Kevin P.; Ton, Dan T.

A Two-layer Distributed Cooperative Control Method for Islanded Networked Microgrid Systems

Xiaoyu Wu, *Student Member, IEEE*, Yin Xu, *Member, IEEE*, Xiangyu Wu, *Member, IEEE*, Jinghan He, *Senior Member, IEEE*, Josep M. Guerrero, *Fellow, IEEE,* Chen-Ching Liu, *Fellow, IEEE*, Kevin P. Schneider, *Senior Member, IEEE* and Dan T. Ton

Abstract—**This paper presents a two-layer distributed cooperative control method for networked microgrid (NMG) systems, taking into account the proprietary nature of microgrid (MG) owners. The proposed control architecture consists of an MG-control layer and an NMG-control layer. In the MG layer, the primary and distributed secondary controls realize accurate power sharing among distributed generators (DGs) and the frequency/voltage reference following within each MG. In the NMG layer, the tertiary control enables regulation of the power flowing through the point of common coupling (PCC) of each MG in a decentralized manner. Furthermore, distributed quaternary control restores the system frequency and critical bus voltage to their nominal values and ensures accurate power sharing among MGs. A small-signal dynamic model is developed to evaluate the dynamic performance of NMG systems with the proposed control method. Time-domain simulations and experiments on NMG test systems are performed to validate the effectiveness of the proposed method.**

Index Terms—**networked microgrids, hierarchical control, distributed cooperative control, resiliency, small-signal stability.**

I. INTRODUCTION

Resiliency against major disasters, such as major hurricanes or earthquakes, is considered by the U.S. Department of Energy (DOE) as the most essential characteristic of future smart distribution systems [1]. Concerning the enhancement of system resiliency, interconnecting microgrids (MGs) to form a networked microgrid (NMG) system after a major outage has

been proved to be an effective option [2].

Three types of NMG systems (or multi-microgrid systems) have been reported in the literature: low-voltage (LV) MGs interconnected through LV tie lines [3], medium-voltage (MV) MGs networked via MV feeders [4], and LV MGs interconnected through an MV feeder and distribution transformers [5], [6]. Disregarding the way in which MGs are networked, NMG systems have some features in common. First, MGs within an NMG system may belong to different entities, and limited information may be shared with others because of their proprietary nature. Second, multiple control objectives need to be realized by effective coordination among DGs and MGs.

A. Literature Review

1) Control architectures of NMG systems

A proper control architecture for NMG systems considering the above features is needed. The classic three-level control architecture [7] is widely applied to a single MG [8]-[14]. The existing control philosophies for NMG systems are usually based on this architecture and fall into two categories, i.e., one-layer architecture and two-layer architecture. The one-layer architecture ignores the boundary of each MG and considers the NMG system as a large MG. Thus, the three-level control architecture of MGs can be modified to fit the NMG system [15]-[17]. The two-layer architecture adds an extra NMG-control layer and considers the three-level control of MGs as the MG-control layer [18]-[31]. The two-layer architecture is inspired by the multi-layer and multi-area control concept in the bulk power system [30]. The NMG layer regards each MG as a control entity and thus avoids directly controlling each DG unit. Therefore, the two-layer architecture is preferred in this study.

However, the existing two-layer architectures have the following limitations: i) they cannot realize load sharing among MGs automatically and enable the plug-and-play capability of each MG, and ii) the NMG-control layer requires too much information of DGs within MGs, which may be inaccessible, e.g., DG capacity information and load consumption data.

2) Control methods of NMG systems

Centralized or distributed methods can both be applied to the control of NMG systems. The centralized control methods for NMG systems have been reported in [19]-[26]. In [19], the NMG layer is responsible for calculating power and voltage reference values and then sending them to the MG layer to realize power sharing and voltage control objectives. In [20],

the frequency control issue is addressed in the NMG layer by coordinating each MG. In [21-26], an interface converter is assumed to be deployed with each MG to realize power sharing among MGs. Thus, the NMG layer is actually responsible for the control of the interfaced converter.

Compared with centralized methods, the distributed control methods employing consensus-based cooperative control theory [33] have some advantages, e.g., communication failure robustness and good re-configurability due to their neighboring communication features. Therefore, they have attracted much attention in recent years.

Among the existing publications with distributed control methods [15], [16], [27]-[29], both one-layer architecture [15], [16] and two-layer architecture have been adopted [27]-[29]. In [15], [16], a distributed communication network including all DG units of the NMG system exists under a one-layer architecture. Thus, there will be a large and complex communication network, which may result in a slow convergence speed of the distributed control algorithm. In [27], [28], the NMG layer is distributed, while the MG layer is still centralized. Thus, the DG units cannot flexibly plug in or out because of the centralized MG layer. In [29], both the MG and NMG layer use distributed control methods. However, MG output power sharing and critical bus voltage control objectives cannot be realized.

In sum, the above methods cannot simultaneously realize the control objectives of both the NMG layer (frequency/voltage regulation and power sharing among MGs) and the MG layer (load sharing among DGs), especially under the two-layer distributed control architecture.

3) Stability modeling and analysis of NMG systems

Compared with a single MG, the dynamic interactions among MGs and among multiple control layers in an NMG system may introduce new low-damping oscillation modes that may even destabilize the system. Therefore, a small-signal dynamic model of the NMG system and its corresponding stability analysis are of significant importance. However, only several publications about the small-signal stability issues of NMG systems have been reported [25], [26], [32]. In [25], [26], a small-signal dynamic modeling method for the NMG system is proposed in which each MG is simplified as a DG unit without considering its internal dynamics. This simplification will inevitably lead to analysis errors. In [32], a detailed small-signal dynamic model of a PV-based NMG is proposed, and the analysis results indicate that the coupling among MGs will weaken the system stability margin. However, only decentralized primary control is employed with each DG in [32], which means the impacts of distributed control methods and other control layers are not studied in [32].

Based on the above analysis, to the best of the authors' knowledge, a detailed small-signal dynamic model and corresponding stability analysis of the NMG system considering distributed control methods and multiple control layers have not been previously reported.

B. Contribution

Compared with the state of the art, the major contributions of this paper are threefold:

1) A two-layer, four-level distributed cooperative control architecture is proposed. In this architecture, each MG is represented by an agent, and only the total spare power capacity information is provided to the NMG layer. Thus, proprietary information of the MG entities is well protected. In addition, an interface level is designed in the NMG layer, which can realize load sharing among MGs automatically as well as enable the plug-and-play capability of each MG.

2) In the NMG-control layer, a control method for the interface level is proposed, and a distributed cooperative control strategy based on it is developed. In the MG-control layer, the classic MG distributed control is adjusted to accommodate the NMG layer. The proposed control strategy is capable of simultaneously i) regulating system frequency and critical bus voltage to desired values and ii) achieving accurate active and reactive power sharing among MGs as well as among DGs within each MG.

3) A unified small-signal dynamic model of the NMG system with the proposed control strategy is constructed. The model is sufficiently detailed, which means the dynamics of every line and load, especially the two-layer distributed cooperative controllers, are included. Moreover, the stability analysis based on the proposed model reveals the newly introduced low-damping oscillation modes and their impact factors. Then, general guidelines are provided for controller parameter tuning based on the stability assessment results.

C. Paper Organization

The remainder of this paper is organized as follows. The proposed control architecture is introduced in Section II. In Section III, the design of controllers and corresponding coordination principles are presented. Section IV develops a unified small-signal dynamic model of a test NMG system. Stability analysis and numerical simulation results are discussed in Section V. Section VI provides the experimental results. Conclusions are summarized in Section VII.

II. THE HIERARCHICAL CONTROL ARCHITECTURE

In this section, the control objectives and overall control architecture for NMG systems are described.

A. Control Objectives

This paper presents a hierarchical architecture to perform frequency and voltage regulation and power sharing control of the NMG system. The control objectives include the following:

(i) To maintain the system frequency f_{sys} at its rated value f_{sys}^*.

(ii) To restore the critical bus voltage V_c to the desired value V_c^*. Note that only one critical bus is assumed, and it can be selected according to the operation requirement.

(iii) To share active and reactive power among MGs in proportion to the reference values, i.e.,

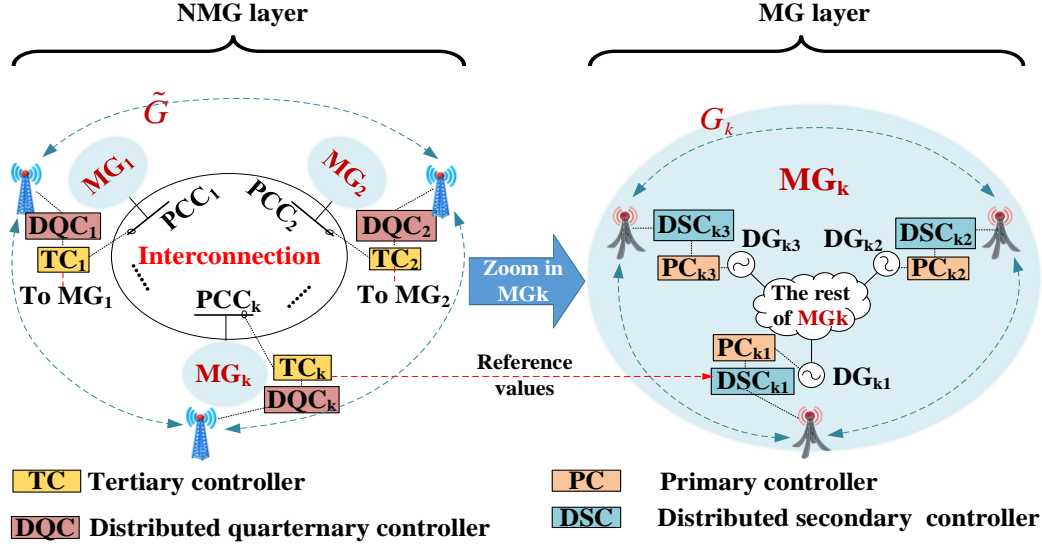$$\frac{1}{P_{PCC1}^*}P_{PCC1} = \frac{1}{P_{PCC2}^*}P_{PCC2} = \cdots = \frac{1}{P_{PCCm}^*}P_{PCCm} \qquad (1)$$

Fig. 1 A schematic diagram of a NMG system with the proposed strategy

$$\frac{1}{Q^*_{\mathrm{PCC1}}} Q_{\mathrm{PCC1}} = \frac{1}{Q^*_{\mathrm{PCC2}}} Q_{\mathrm{PCC2}} = \cdots = \frac{1}{Q^*_{\mathrm{PCC}m}} Q_{\mathrm{PCC}m} \qquad (2)$$

where $P^*_{\mathrm{PCC}k}$, $Q^*_{\mathrm{PCC}k}$, $P_{\mathrm{PCC}k}$, and $Q_{\mathrm{PCC}k}$ are the active and reactive power references for the point of common coupling (PCC) of MG$_k$ and the output active and reactive power of PCC$_k$, respectively, with $k \in \mathcal{M}$, $\mathcal{M} = \{1, 2, \ldots, m\}$. In this paper, $P^*_{\mathrm{PCC}k}$ and $Q^*_{\mathrm{PCC}k}$ are equal to the active and reactive capacity of MG$_k$, denoted by $P_{\mathrm{maxMG}k}$ and $Q_{\mathrm{maxMG}k}$, respectively. Note that $P^*_{\mathrm{PCC}k}$ and $Q^*_{\mathrm{PCC}k}$ can also be determined according to optimal power flow results, which makes the control objectives flexible. Equations (1) and (2) are denoted as objective (iii)-(1) and objective (iii)-(2), respectively.

(iv) Within each MG, active and reactive power can be shared among DGs based on their power capacities, i.e.,

$$\frac{1}{P_{\mathrm{max}k1}} P_{k1} = \frac{1}{P_{\mathrm{max}k2}} P_{k2} = \cdots = \frac{1}{P_{\mathrm{max}kn_k}} P_{kn_k} \qquad (3)$$

$$\frac{1}{Q_{\mathrm{max}k1}} Q_{k1} = \frac{1}{Q_{\mathrm{max}k1}} Q_{k2} = \cdots = \frac{1}{Q_{\mathrm{max}kn_k}} Q_{kn_k} \qquad (4)$$

where $P_{\mathrm{max}ki}$, $Q_{\mathrm{max}ki}$, P_{ki} and Q_{ki} are active and reactive power capacities and active and reactive power outputs of DG$_i$ in MG$_k$, respectively, with $i \in \mathcal{N}_k$, $\mathcal{N}_k = \{1, 2, \ldots, n_k\}$. Equations (3) and (4) are denoted as objective (iv)-(1) and objective (iv)-(2), respectively.

In our previous work [6], an NMG power flow model considering the above objectives is proposed, and only one solution exists, which demonstrates that the objectives (i)~(iv) can be met simultaneously.

B. The Proposed Two-Layer Control Architecture

To realize the aforementioned control objectives, a two-layer control architecture is proposed, as shown in Fig. 1. There are m MGs in the system, marked as MG$_1$, MG$_2$,…, MG$_k$, …, MG$_m$. In the NMG-control layer, each MG is modeled as an agent to form the upper distributed communication network $\tilde{G}$. Each MG agent includes a distributed quarternary controller (DQC) and a tertiary controller (TC). The DQC exchanges information

with its neighbors to generate control variables and sends them to the corresponding TC to realize NMG layer control objectives. In the MG-control layer, MG$_k$ is selected and magnified to present the MG-layer control. In MG$_k$, all the DG units are assumed to be communication nodes to form a lower communication network G_k. Each DG unit deploys a distributed secondary controller (DSC) and a primary controller (PC). The DSC communicates with its neighbors to generate control variables and sends them to the corresponding PC to realize MG layer control objectives.

Note that the dotted lines with arrows represent directed communication links. Each TC sends commands to a DSC in the corresponding MG to realize interactions between upper and lower communication networks, as shown by the red dotted link.

1) MG-control layer: This layer aims at meeting the frequency, voltage and power sharing control objectives of the MG layer as well as supporting the NMG layer control.

a) The *primary controller (PC) level* is responsible for regulating the output power of DGs via the droop method [11].

b) The *distributed secondary controller (DSC) level* is responsible for regulating the MG frequency and PCC voltage according to the reference values received from the tertiary controller level. The control actions are taken by sending compensation signals to the primary controllers.

2) NMG-control layer: This layer handles the control of system frequency and critical bus voltage as well as power sharing among MGs.

c) The *tertiary controller (TC) level* is responsible for sharing power among MGs by controlling the PCC power flow according to the droop characteristics. By adjusting the frequency and PCC voltage reference values, which are sent to the distributed secondary level, the PCC power flow is controlled. Note that only the total spare capacity information of MGs is needed at this level.
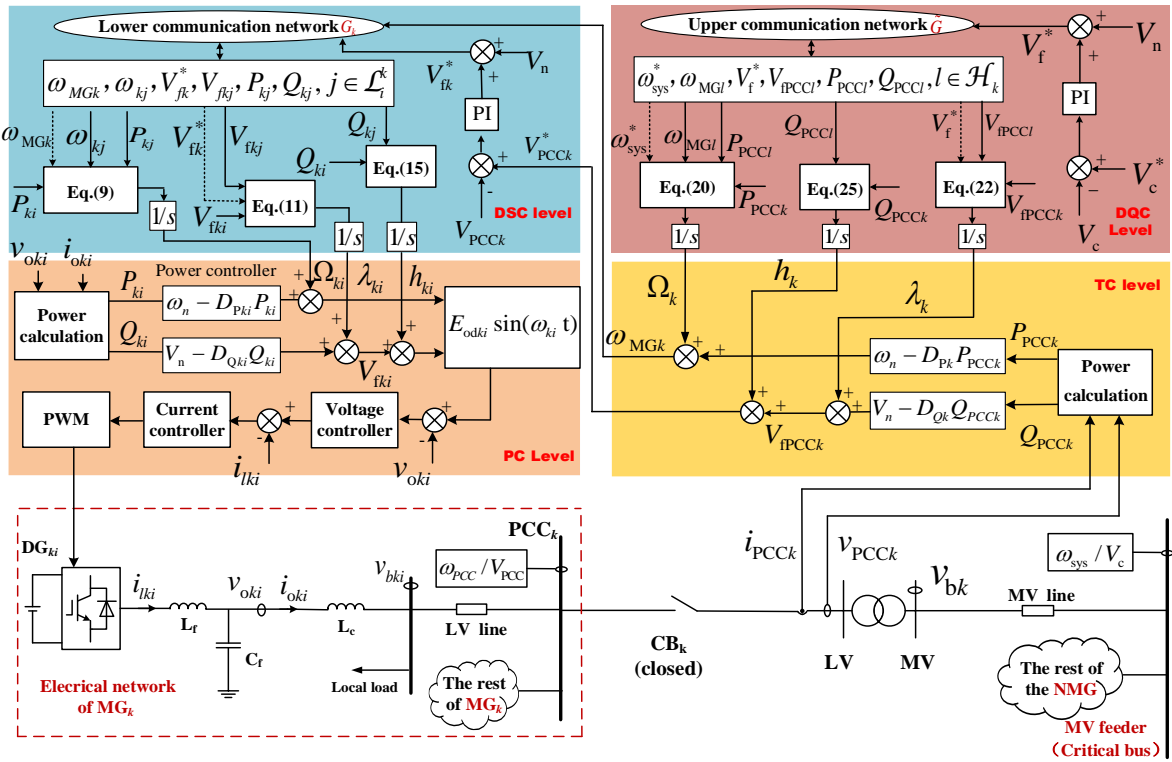
Fig. 2 A block diagram of the proposed two-layer distributed cooperative control method

d) The *distributed quaternary controller (DQC) level* regulates the system frequency and critical bus voltage to their desired values by coordinating MGs in a distributed manner.

In sum, the proposed architecture has the following advantages: i) only the spare capacity information of each MG is needed by the NMG layer, which well respects the proprietary nature of MG entities; ii) the TC level can realize load sharing among MGs automatically; iii) the two-layer distributed feature enables the plug-and-play of both DG and MG unit.

III. CONTROLLER DESIGN

Based on the proposed architecture, the corresponding controllers and coordination strategy are described in this section. Fig. 2 shows the control block diagram of an NMG system. To simplify the description, MG_k and its inside DG_{ki} are selected to present the control principles. DG_{ki} is employed with an LCL filter and a local load and then connects with the PCC bus of MG_k through an LV line. For MG_k, the system connects with the MV critical bus through the circuit breaker CB_k, LV/MV distribution transformer and an MV line.

In Fig. 2, the red and yellow blocks on the right present control strategies of DQC and TC in the NMG-control layer for MG_k. The blue and orange blocks on the left present control strategies of DSC and PC in the MG-control layer for DG_{ki}. Detailed control principles will be described in the following subsections. Note that the proposed control is also suitable for other types of NMG systems introduced in Section I.

A. PC Level

At this level, the droop-based control is adopted, which

consists of the power controller, inner voltage controller and current controller, as shown in Fig. 2. The power controller allows DGs to share active and reactive power demand based on their power capacities by setting droop coefficients, i.e.,

$$\omega_{ki} = \omega_{\mathrm{n}} - D_{\mathrm{P}ki}P_{ki} \tag{5}$$

$$V_{fki} = V_{\mathrm{n}} - D_{\mathrm{Q}ki}Q_{ki} \tag{6}$$

where ω_{ki} is the angular frequency of DG_i in MG_k, ω_{n} is the rated angular frequency, V_{n} is the rated voltage of the LV network, and V_{fki} is the inverter AC-side voltage reference provided to the inner voltage controller. $D_{\mathrm{P}ki}$ and $D_{\mathrm{Q}ki}$ are the active and reactive power droop coefficients, given by

$$D_{\mathrm{P}ki} = \frac{\omega_{\max}-\omega_{\min}}{P_{\max ki}}, \quad D_{\mathrm{Q}ki} = \frac{V_{\max}-V_{\min}}{Q_{\max ki}} \tag{7}$$

where $\omega_{\max}$ and $\omega_{\min}$ are the upper and lower limits of the angular frequency, respectively. $V_{\max}$ and $V_{\min}$ are the upper and lower limits of the DG output voltage, respectively.

B. DSC Level

The DSC level is responsible for realizing the power-sharing objectives of DGs within each MG as well as tracking the voltage and frequency reference values from the tertiary level. The consensus-based distributed cooperative control theory [33] is used to design the DSC. The term "distributed" means that each agent only needs its own information and that of its neighbors in a distributed communication network to update its state. The term "cooperative" means that all agents work as a group to realize a common synchronization goal. Based on the continuous consensus algorithm, the states of all the agents will synchronize to a common value in the steady state, i.e., they reach a "consensus".

The communication network in this level contains m di-

graphs, $G_1, G_2 \ldots G_m$, corresponding to m MGs, respectively. For MG_k, the set of neighbors of DG node i is denoted as $\mathcal{L}_i^k$. Each node requires its own information and that of its neighbor j ($j \in \mathcal{L}_i^k$) on the digraph to update its states. The associated adjacency matrix is $\mathbf{A}^k = [a_{ij}^k]$. Details of the communication network at this level are provided in the Appendix.

1) Distributed secondary frequency control: With this control, objectives (iv)-(3) can be achieved. In addition, the frequency reference value ω_{MGk} from TC_k can be tracked. The reference value ω_{MGk} for different MGs can be different during transient events to adjust the PCC power flow but will converge to the system rated angular frequency ω_{sys}^* when the system reaches a steady state. The controller design is a combination of the regulator synchronization problem [33] and the tracking synchronization problem [34], given by

$$\omega_{ki} = \omega_n - D_{Pki}P_{ki} + \Omega_{ki} \qquad (8)$$

$$\frac{d\Omega_{ki}}{dt} = -c_{\omega ki}\left[\sum_{j \in \mathcal{L}_i^k} a_{ij}^k(\omega_{ki} - \omega_{kj}) + g_i^k(\omega_{ki} - \omega_{MGk})\right]$$
$$- c_{pki}\sum_{j \in \mathcal{L}_i^k} a_{ij}^k(D_{Pki}P_{ki} - D_{Pkj}P_{kj}) \qquad (9)$$

where $c_{\omega ki}$ and c_{pki} are the positive control gains, and the pinning gain $g_i^k \geq 0$ is the weight of the edge connected to the reference. It is non-zero only for a few nodes (at least one node). Equation (8) is transformed from (5) with an additional DSC variable Ω_{ki}.

2) Distributed secondary PCC voltage control: This controller is responsible for controlling each MG's PCC voltage to the reference V_{PCCk}^* from TC_k. The correction term λ_{ki} is added in the reactive power droop control (6), i.e.,

$$V_{fki} = V_n - D_{Qki}Q_{ki} + \lambda_{ki} \qquad (10)$$

$$\frac{d\lambda_{ki}}{dt} = -c_{vki}[\sum_{j \in \mathcal{L}_i^k} a_{ij}^k(V_{fki} - V_{fkj}) + g_i^k(V_{fki} - V_{fk}^*)] \quad (11)$$

where c_{vki} is a positive control gain. $\sum_{j \in \mathcal{L}_i^k} a_{ij}^k(V_{fki} - V_{fkj}) + g_i^k(V_{fki} - V_{fk}^*)$ is the local neighbor tracking error of V_{fki}, which enables voltage regulation. V_{fk}^* is generated through a PI controller such that V_{PCCk} recovers to its reference V_{PCCk}^*, which is received from TC_k, i.e.,

$$V_{fk}^* = V_n + k_{pk}(V_{PCCk}^* - V_{PCCk})$$
$$+ k_{ik}\int(V_{PCCk}^* - V_{PCCk})\,dt \qquad (12)$$

where k_{pk} and k_{ik} are the gains of the PI controller.

3) Distributed secondary reactive power control: This controller addresses the inaccuracy of the reactive power sharing problem due to the unbalanced line impedance [10]. Thus, the voltage correction term h_{ki} is added to the right-hand side of (10) to realize accurate reactive power sharing among DGs within MG_k, namely, objective (iv)-(4), by regulating the voltage reference, i.e.,

$$E_{odki} = \overbrace{V_n - D_{Qki}Q_{ki} + \lambda_{ki}}^{V_{fki}} + h_{ki} \qquad (13)$$

$$E_{oqki} = 0 \qquad (14)$$

where the voltage reference, i.e., $V_n - D_{Qki}Q_{ki} + \lambda_{ki} + h_{ki}$, is aligned to the d-axis of the DG_{ki} local dq-frame, and the q-axis reference, i.e., E_{oqki}, is set to zero. Then, E_{odki} and E_{oqki} are provided to the inner voltage controller. h_{ki} is selected such that $D_{Qki}Q_{ki}$ of each DG in MG_k converges to a common value, which is a regulator synchronization problem [33] given by

$$\frac{dh_{ki}}{dt} = -c_{qki}\sum_{j \in \mathcal{L}_i^k} a_{ij}^k(D_{Qki}Q_{ki} - D_{Qkj}Q_{kj}) \qquad (15)$$

where c_{qki} is a positive control gain, and $\sum_{j \in \mathcal{L}_i^k} a_{ki}(D_{Qki}Q_{ki} - D_{Qkj}Q_{kj})$ is the local neighbor tracking error that enables accurate reactive power sharing.

C. TC Level

This level is an interface level that can realize load sharing among MGs automatically as well as enable the plug-and-play capability of each MG. In addition, the proprietary information of each MG can be well protected by introducing this level. The droop control is modified to control the output power through the PCC of MGs, i.e.,

$$\omega_{MGk} = \omega_n - D_{Pk}P_{PCCk} \qquad (16)$$

$$V_{fPCCk} = V_n - D_{Qk}Q_{PCCk} \qquad (17)$$

where D_{Pk} and D_{Qk} are the active and reactive droop coefficients of MG_k, respectively, determined by

$$D_{Pk} = \frac{\omega_{max} - \omega_{min}}{P_{maxMGk}}, \quad D_{Qk} = \frac{V_{max} - V_{min}}{Q_{maxMGk}} \qquad (18)$$

At this level, each MG is considered a droop-controlled node, and only the spare power capacity of each MG is needed.

D. DQC Level

The DQC level is responsible for regulating system frequency and critical bus voltage to desired values, as well as realizing accurate power sharing among MGs. The controller at this level is also designed based on consensus-based distributed cooperative control. The communication network in this level is denoted as $\tilde{G}$ with the associated adjacency matrix $\mathbf{A} = [a_{kl}]$. For MG node k, the set of neighbors of node k is denoted as $\mathcal{H}_k$. Three controllers are included in this level. Details of the communication network at this level are given in the Appendix.

1) Distributed quaternary frequency control: With this control, objective (i) and objective (iii)-(1) can be achieved. The controller design is as follows.

$$\omega_{MGk} = \omega_n - D_{Pk}P_{PCCk} + \Omega_k \qquad (19)$$

$$\frac{d\Omega_k}{dt} = -c_{\omega k}\left[\sum_{l \in \mathcal{H}_k} a_k(\omega_{MGk} - \omega_{MGl}) + g_k(\omega_{MGk} - \omega_{sys}^*)\right]$$
$$- c_{pk}\sum_{l \in \mathcal{H}_k} a_k(D_{Pk}P_{PCCk} - D_{Pl}P_{PCCl}) \qquad (20)$$

where $c_{\omega k}$ and c_{pk} are positive control gains. Equation (19) is (16) with an additional quaternary control variable Ω_k. ω_{MGk} is generated as the frequency reference of (9).

2) Distributed quaternary critical bus voltage control: This controller is responsible for achieving objective (ii). The term λ_k is added in MG's reactive power droop controller (17), i.e.,

$$V_{fPCCk} = V_n - D_{Qk}Q_{PCCk} + \lambda_k \qquad (21)$$

$$\frac{d\lambda_k}{dt} = -c_{vk}[\sum_{l \in \mathcal{H}_k} a_{kl}(V_{fPCCk} - V_{fPCCl}) + g_k(V_{fPCCk} - V_f^*)] \qquad (22)$$

where c_{vk} is a positive control gain, and V_f^* is generated through a PI controller such that V_c recovers to its reference V_c^*, i.e.,

$$V_f^* = V_n + k_p(V_c^* - V_c) + k_i\int(V_c^* - V_c)\,dt \qquad (23)$$

where k_p and k_i are the gains of the PI controller.

This article has been accepted for publication in a future issue of this journal, but has not been fully edited. Content may change prior to final publication. Citation information: DOI 10.1109/TSG.2019.2928330, IEEE Transactions on Smart Grid

6

3) Distributed quaternary reactive power control: The inaccurate reactive power sharing among MGs is managed by this controller. The voltage correction term h_k is added to the right side of (21) to achieve accurate reactive power sharing by regulating the voltage reference, i.e.,

$$V_{\text{PCC}k}^* = \overbrace{V_n - D_{\text{Q}k}Q_{\text{PCC}k}}^{V_{\text{fPCC}k}} + \lambda_k + h_k \qquad (24)$$

where the voltage reference $V_{\text{PCC}k}^*$ is generated as the reference of (12). h_k is selected such that $n_k Q_{\text{PCC}k}$ of each MG converges to a common value given by

$$\frac{dh_k}{dt} = -c_{\text{q}k}\sum_{l\in\mathcal{L}_k} a_{kl}\big(D_{\text{Q}k}Q_{\text{PCC}k} - D_{\text{Q}l}Q_{\text{PCC}l}\big) \qquad (25)$$

where $c_{\text{q}k}$ is a positive control gain. Thus, objective (iii)-(2) can be realized.

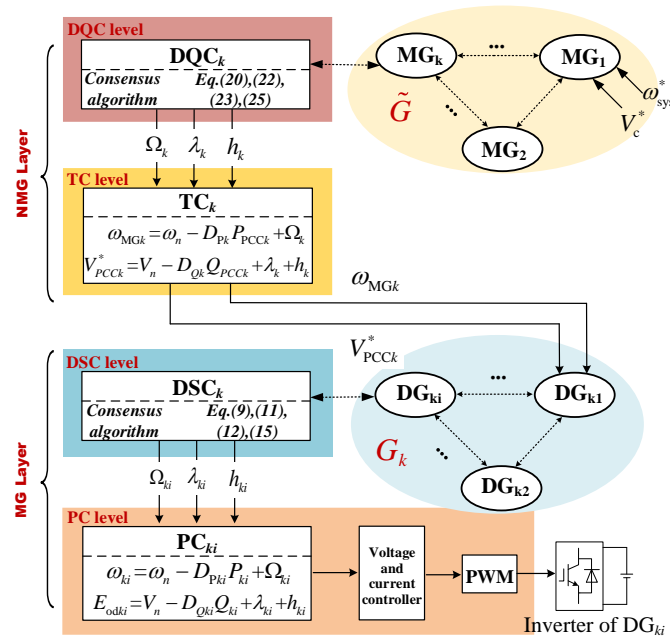*E. Flow chart and implementation steps of the proposed method*

Fig. 3 Flow chart of the proposed control method

To illustrate the execution process of the proposed method. A flow chart diagram is shown in Fig. 3. In addition, the corresponding implementation steps are given as follows:

Step 1 (DQC level): The rated system frequency ω_{sys}^* and desired critical bus voltage V_c^* are transmitted to agent MG$_1$ in the upper communication network $\tilde{G}$. Through the distributed consensus algorithm (20), (22), (23) and (25), the control variables Ω_k, λ_k and h_k are obtained and sent to TC level;

Step 2 (TC level): The TC is a droop-based controller that is used to adjust the PCC power flow of each MG. Ω_k is applied to shift the frequency-active power droop curve to realize objective (i) and objective (iii)-(1). λ_k and h_k are applied to shift the voltage-reactive power droop curve to realize objective (ii) and objective (iii)-(2). The output variables $\omega_{\text{MG}k}$ and $V_{\text{PCC}k}^*$ are sent to DSC level;

Step 3 (DSC level): $\omega_{\text{MG}k}$ and $V_{\text{PCC}k}^*$ are received by DG$_{k1}$ in the lower communication network G_k. Through the distributed

consensus algorithms (9), (11), (12) and (15), the control variables Ω_{ki}, λ_{ki} and h_{ki} are obtained and sent to PC level;

Step 4 (PC level): PC is droop-based for each DG unit. Ω_{ki} regulates the angular frequency of DG$_{ki}$ to $\omega_{\text{MG}k}$ and realizes objective (iv)-(1) by shifting the frequency-active power droop curve of PC. λ_{ki} and h_{ki} regulate the output voltage of DG$_{ki}$ to $V_{\text{f}k}^*$ and realize objective (iv)-(2). The output frequency reference ω_{ki} and voltage reference $E_{\text{od}ki}$ are sent to the voltage and current controller, and the switching signals through the PWM module are finally generated to control the inverter of DG$_{ki}$.

In sum, with the proposed two-layer distributed cooperative control method, the multiple control objectives summarized in section II-A can be coordinated and simultaneously realized.

IV. Small-Signal Dynamic Model of NMG Systems

The existing works on small-signal dynamic modeling of NMG systems have the limitations of i) oversimplification of MG's internal dynamics [25], [26] and ii) omission of multiple control levels and distributed controllers in modeling [32]. Thus, the stability analysis based on these models will inevitably introduce errors. To accurately reveal the dynamic interaction mechanism and evaluate the dynamic performance of the proposed method, this section develops a detailed small-signal dynamic model of the NMG system in Fig. 2.

A. MG Layer Modeling

The MG layer model represents the dynamics of the PC and DSC controllers as well as the lines and loads within MGs. Note that each MG is modeled separately and will be combined in Section IV-C.

1) DG unit model: In this paper, the local dq-frame of DG$_{11}$, namely, DG$_1$ in MG$_1$, is selected as the common DQ-frame. The symbol ω_g denotes the rotating frequency of DQ-frame and $\omega_g = \omega_{11}$. δ_{ki} is the angle between the local dq-frame of DG$_{ki}$ and the common DQ-frame, and then

$$\dot{\delta}_{ki} = \omega_{ki} - \omega_{\text{g}} \qquad (26)$$

This paper focuses on the dynamics of the power controller. Therefore, the relatively fast dynamics of voltage and current controllers can be neglected by assuming

$$v_{\text{od}ki} = E_{\text{od}ki}, \ v_{\text{oq}ki} = E_{\text{oq}ki} \qquad (27)$$

where $v_{\text{od}ki}$ and $v_{\text{oq}ki}$ are the d-axis and q-axis component of DG output voltage $v_{\text{o}ki}$, respectively, as shown in Fig. 2.

By linearizing (8)-(11), (13)-(15) and (26) around an operating point, the model of DG$_{ki}$ can be derived as

$$\begin{aligned}[\Delta\dot{X}_{\text{DG}ki}] = &A_{\text{DG}ki}[\Delta X_{\text{DG}ki}] + B_{\text{DG}ki}[\Delta v_{\text{bDQ}ki}] + C_{\text{DG}ki}\Delta\omega_{\text{g}} + \\ &\sum_{j\in\mathcal{L}_i^k} F_{\text{DG}ki}[\Delta X_{\text{DG}kj}] + H_{\text{DG}ki}\Delta V_{\text{f}k}^* \qquad (28)\end{aligned}$$

where $\Delta v_{\text{bDQ}ki}$ is the deviation of $v_{\text{b}ki}$ (bus voltage as shown in Fig. 2) in the common DQ-frame, and $A_{\text{DG}ki}$, $B_{\text{DG}ki}$, $C_{\text{DG}ki}$, $F_{\text{DG}ki}$ and $H_{\text{DG}ki}$ are parameter matrices. Note that $F_{\text{DG}ki}$ reflects the correlation between DG$_{ki}$ and its neighbors DG$_{kj}$, $j \in \mathcal{L}_i^k$. The state variables of each DG unit are

$$[\Delta X_{\text{DG}ki}] = \big[\Delta\delta_{ki}, \Delta P_{ki}, \Delta Q_{ki}, \Delta\Omega_{ki}, \Delta\lambda_{ki}, \Delta h_{ki}, \Delta i_{\text{od}ki}, \Delta i_{\text{oq}ki}\big]^T \qquad (29)$$

2) PCC voltage controller model: Introduce ψ_k as the state variable to describe the dynamics of (12), i.e.,

$$\dot{\psi}_k = V^*_{\text{PCC}k} - V_{\text{PCC}k} \tag{30}$$

where $V_{\text{PCC}k} = \sqrt{V^2_{\text{PCCD}k} + V^2_{\text{PCCQ}k}}$. Then, the small-signal dynamic model of the PCC voltage controller is obtained by linearizing (30) and (12), i.e.,

$$\Delta\dot{\psi}_k = -A_{\text{PCC}k}[\Delta V_{\text{PCCDQ}k}] + \Delta V^*_{\text{PCC}k} \tag{31}$$

$$\Delta V^*_{\text{f}k} = -k_{\text{p}k}A_{\text{PCC}k}[\Delta V_{\text{PCCDQ}k}] + k_{\text{p}k}\Delta V^*_{\text{PCC}k} + k_{\text{i}k}\Delta\psi_k \tag{32}$$

where $\Delta V_{\text{PCCDQ}k} = [\Delta V_{\text{PCCD}k}, \Delta V_{\text{PCCQ}k}]^T$, and $A_{\text{PCC}k}$ is the parameter matrix.

3) Network and load models within MG_k: The network and load models [9] are developed based on the lumped, series RL feeder lines and the RL-type constant-impedance loads, respectively, i.e.,

$$\Delta i_{\text{lineDQ}k} = A_{\text{net}k}[\Delta i_{\text{lineDQ}k}] + B_{\text{net}k}[\Delta v_{\text{bDQ}k}] + C_{\text{net}k}\Delta\omega_{\text{g}} \tag{33}$$

$$\Delta i_{\text{loadDQ}k} = A_{\text{load}k}[\Delta i_{\text{loadDQ}k}] + B_{\text{load}k}[\Delta v_{\text{bDQ}k}] + C_{\text{load}k}\Delta\omega_{\text{g}} \tag{34}$$

where $\Delta i_{\text{lineDQ}k}$, $\Delta i_{\text{loadDQ}k}$ and $\Delta v_{\text{bDQ}k}$ are variables of all lines, loads and bus voltages within MG_k, respectively. The deviation of $i_{\text{o}ki}$ of all the DG units and $i_{\text{PCC}k}$ of MG_k, shown in Fig. 2, is denoted as $\Delta i_{\text{oDQ}k}$ and $\Delta i_{\text{PCCDQ}k}$ in the common DQ-frame, respectively. Then, $\Delta v_{\text{bDQ}k}$ is represented as [9]

$$\Delta v_{\text{bDQ}k} = R_N(M_{\text{DG}k}[\Delta i_{\text{oDQ}k}] + M_{\text{net}k}[\Delta i_{\text{lineDQ}k}] + M_{\text{load}k}[\Delta i_{\text{loadDQ}k}] + M_{\text{PCC}k}[\Delta i_{\text{PCCDQ}k}]) \tag{35}$$

Since PCC_k is also a bus within MG_k, $\Delta V_{\text{PCCDQ}k}$ can be expressed in terms of $\Delta i_{\text{oDQ}k}$, $\Delta i_{\text{lineDQ}k}$, $\Delta i_{\text{loadDQ}k}$, $\Delta i_{\text{PCCDQ}k}$ and named $\Delta V_{\text{PCCDQ}k}$ *expression*.

4) The complete model of MG_k: Use the state variables of all DG units within MG_k as ΔX_{DGk}, then combine (28), (31), (33), (34) and replace ΔV^*_{fk}, Δv_{bQk}, ΔV_{PCCDQk} with (32), (35) and ΔV_{PCCDQk} expression, respectively. The small-signal dynamic model of MG_k is obtained, i.e.,

$$[\Delta\dot{S}_{\text{MG}k}] = A_{\text{MG}k}[\Delta S_{\text{MG}k}] + B_{\text{MG}k}\Delta V^*_{\text{PCC}k} + C_{\text{MG}k}[\Delta i_{\text{PCCDQ}k}] \tag{36}$$

where $\Delta S_{\text{MG}k} = [\Delta X_{\text{DG}k}, \Delta i_{\text{lineDQ}k}, \Delta i_{\text{loadDQ}k}, \Delta\psi_k]^T$, $A_{\text{MG}k}, B_{\text{MG}k}$ and $C_{\text{MG}k}$ are parameter matrices.

B. NMG Layer Modeling

The NMG layer modeling covers the dynamics of TC and DQC controllers as well as MV lines and loads. Note that each MG will be viewed as a black box and referred to as an MG unit.

1) MG unit model: By linearizing (19)-(22), (24)-(25) around an operating point, the model of MG_k becomes

$$[\Delta\dot{X}_{\text{MG}k}] = A_{\text{MG}k}[\Delta X_{\text{MG}k}] + B_{\text{MG}k}[\Delta v_{\text{bDQ}k}] + C_{\text{MG}k}\Delta\omega_{\text{g}} + \sum_{l\in\mathcal{H}_k}F_{\text{MG}k}[\Delta X_{\text{MG}l}] + H_{\text{MG}k}\Delta V^*_{\text{f}} + I_{\text{MG}k}[\Delta V_{\text{PCCDQ}k}] \tag{37}$$

where $\Delta v_{\text{bDQ}k}$ is the deviation of MV bus voltage $v_{\text{b}k}$ in the common DQ-frame, and $A_{\text{MG}k}, B_{\text{MG}k}\ C_{\text{MG}k}, F_{\text{MG}k}$ and $H_{\text{MG}k}$

are parameter matrices. Note that $F_{\text{MG}k}$ reflects the correlation between unit MG_k and its neighbors MG_l, $l \in \mathcal{H}_k$. The state variables of each MG unit are

$$[\Delta X_{\text{MG}k}] = [\Delta\delta_k, \Delta P_{\text{PCC}k}, \Delta Q_{\text{PCC}k}, \Delta\Omega_k, \Delta\lambda_k, \Delta h_k, \Delta i_{\text{PCCd}k}, \Delta i_{\text{PCCq}k}]^T \tag{38}$$

2) Critical bus voltage controller model: Denote ψ as the state of (23), i.e.,

$$\dot{\psi} = V^*_{\text{c}} - V_{\text{c}} \tag{39}$$

where $V_{\text{c}} = \sqrt{V^2_{\text{cD}} + V^2_{\text{cQ}}}$. By linearizing (23) and (39), the model of the critical bus voltage controller can be obtained:

$$\Delta\dot{\psi} = -A_{\text{c}}[\Delta V_{\text{cDQ}}] \tag{40}$$
$$\Delta V^*_{\text{f}} = -k_{\text{p}}A_{\text{c}}[\Delta V_{\text{cDQ}}] + k_{\text{i}}\Delta\psi \tag{41}$$

where $\Delta V_{\text{cDQ}} = [\Delta V_{\text{cD}}, \Delta V_{\text{cQ}}]^T$, and A_{c} is the parameter matrix.

3) MV network and load models: The modeling of the MV network and load is the same as that in MG layer modeling and can be expressed as

$$\Delta i_{\text{lineDQ}} = A_{\text{net}}[\Delta i_{\text{lineDQ}}] + B_{\text{net}}[\Delta v_{\text{bDQ}}] + C_{\text{net}}\Delta\omega_{\text{g}} \tag{42}$$

$$\Delta i_{\text{loadDQ}} = A_{\text{load}}[\Delta i_{\text{loadDQ}}] + B_{\text{load}}[\Delta v_{\text{bDQ}}] + C_{\text{load}}\Delta\omega_{\text{g}} \tag{43}$$

where Δi_{lineDQ}, Δi_{loadDQ} and Δv_{bDQ} are variables of MV lines, loads and buses, respectively. Δi_{PCCDQ} denotes $\Delta i_{\text{PCCDQ}k}$ of all the MG units. Then, Δv_{DQ} is represented as

$$\Delta v_{\text{bDQ}} = R_N(M_{\text{MG}}[\Delta i_{\text{PCCDQ}}] + M_{\text{net}}[\Delta i_{\text{lineDQ}}] + M_{\text{load}}[\Delta i_{\text{loadDQ}}]) \tag{44}$$

Since the critical bus is also an MV bus, ΔV_{cDQ} can be expressed in terms of Δi_{PCCDQ}, Δi_{lineDQ} and Δi_{loadDQ} and named ΔV_{cDQ} *expression*.

4) Complete the NMG layer model: Denote the state variables of all MG units in the NMG system as ΔX_{MG}. Combine (37), (40), (42), (43) and replace ΔV^*_f, Δv_{bDQ}, ΔV_{cDQ} with (41), (44) and ΔV_{cDQ} *expression*. Then, the small-signal dynamic model of the NMG layer is obtained. That is,

$$[\Delta\dot{S}_{\text{NMG}}] = A_{\text{NMG}}[\Delta S_{\text{NMG}}] + B_{\text{NMG}}\Delta V_{\text{PCCDQ}k} \tag{45}$$

where $\Delta S_{\text{NMG}} = [\Delta X_{\text{MG}}, \Delta i_{\text{lineDQ}}, \Delta i_{\text{loadDQ}}, \Delta\psi]^T$, A_{NMG} and B_{NMG} are parameter matrices.

C. Complete NMG System Model

In (36) and (45), the coupling states $\Delta V^*_{\text{PCC}k}$, $\Delta i_{\text{PCCDQ}k}$ and $\Delta V_{\text{PCCDQ}k}$ can be dealt with as follows: i) linearize (24), and then $\Delta V^*_{\text{PCC}k}$ in (36) can be represented by $\Delta X_{\text{MG}k}$ in (38), which is part of ΔS_{NMG}; ii) represent $\Delta i_{\text{PCCDQ}k}$ by $\Delta X_{\text{MG}k}$, which is part of ΔS_{NMG}, and iii) replace $\Delta V_{\text{PCCDQ}k}$ by $\Delta V_{\text{PCCDQ}k}$ *expression*, which is then represented by ΔS_{MG}. By combining m MG layer models (36) and the NMG layer model (45), the complete NMG system model can be obtained as
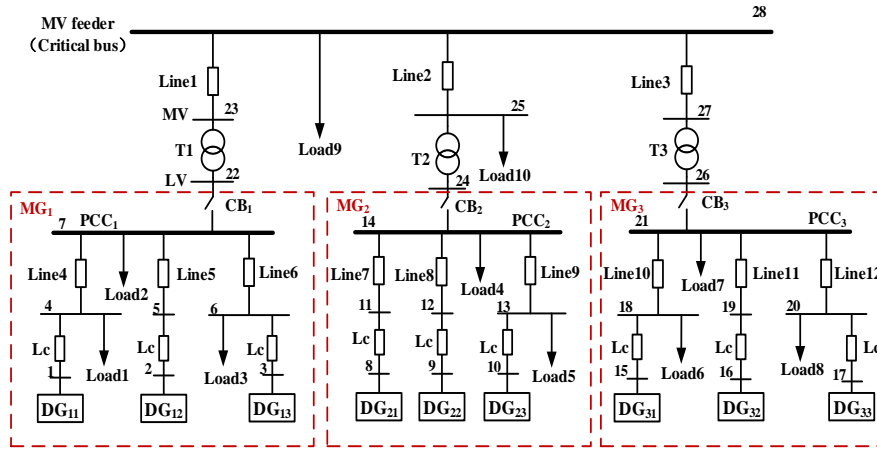
Fig. 4 A schematic diagram of the test NMG system

$$\left[\Delta \dot{S}_{\text{sys}}\right] = A_{\text{sys}}\left[\Delta S_{\text{sys}}\right] \qquad (46)$$

where $\Delta S_{\text{sys}} = [\Delta S_{\text{MG1}}, \ldots, \Delta S_{\text{MGm}}, \Delta S_{\text{NMG}}]^T$. A_{sys} is the state matrix of the NMG system.

V. NUMERICAL STUDY

To validate the effectiveness of the proposed two-layer distributed control method, stability analyses and time-domain simulation studies in the PSCAD/EMTDC platform are carried out in this section based on a test NMG system.

A. Test System

The test NMG system consisting of 3 MGs is shown in Fig. 4. The circuit breakers (CB) 1, 2 and 3 are closed. The rated voltages of the MV and LV networks are 10 kV and 0.38 kV, respectively. MG$_1$ and MG$_3$ include 3 DGs, 3 LV lines and 3 loads. MG$_2$ includes 3 DGs, 3 LV lines and 2 loads. L_c is the coupling inductance. Each MG connects with the MV feeder through a 10 kV/0.38 kV Δ/Y_g transformer. The MV feeder is regarded as the critical bus. Tables I, II and III provide the system and controller parameters.

TABLE I. ELECTRICAL PARAMETERS OF THE NMG SYSTEM

Line	Line 1: 0.08 + j0.12 Ω. Line 2: 0.05 + j0.07 Ω, Line 3: 0.07 + j0.11 Ω, Lines 4,8,10,11: 0.15 + j0.05 Ω, Lines 6,7,12: 0.11 + j0.07 Ω, Lines 5,9: 0.11 + j0.11 Ω,
Load	Load 9 = 100 kw + 30 kvar, Load 10 = 20 kw + 5 kvar, Loads 1,5,8 = 15 kw + 7.5 kvar, Loads 3,6 = 12 kw + 5 kvar, Load 2 = 40 kw + 15 kvar, Loads 4,7 = 50 kw + 20 kvar
Transformer	T1/T2/T3: 1MVA, u_k = 4%, r_k = 1%, 10/0.38 KV(Δ/Y_g)

TABLE II. PARAMETERS OF PCS AND TCS

Parameters	DG$_{11}$ DG$_{12}$ DG$_{13}$ DG$_{31}$ DG$_{32}$ DG$_{33}$	DG$_{21}$DG$_{22}$ DG$_{23}$	MG$_1$ MG$_3$	MG$_2$
D_{Pki}/D_{Pk} (Hz/kW · 10^{-3})	16.67	20	5.56	6.67
D_{Qki}/D_{Qk} (kV/kvar · 10^{-3})	0.78	0.52	0.26	0.173
$P_{\max}/P_{sMG}$ (kW)	60	50	180	150
$Q_{\max}/Q_{sMG}$ (kvar)	20	30	60	90

TABLE III. PARAMETERS OF DSCS AND DQCS

Parameters	DSC level	DQC level
$c_{\omega ki}/c_{\omega k}$	490	1252
c_{pki}/c_{pk}	65	3242
c_{vki}/c_{vk}	98	43
c_{qki}/c_{qk}	40	26
k_{pk}/k_p	30	5
k_{ik}/k_i	0.05	20

Reference values of the system frequency and critical bus voltage are given as $f_{\text{sys}}^* = 50$ Hz and $V_c^* = 1$ p.u., respectively. The communication networks $\tilde{G}$ for the NMG layer and G_k for the MG layer are assumed to have the same topology as shown in Fig. 5. From Fig. 5, MG agents and DG agents can communicate with their neighbors through communication links (arrowed and dotted lines). In $\tilde{G}$, MG$_1$ receives the reference value ($\omega_{\text{sys}}^*/V_f^*$) with pinning gain $g_1 = 1$. Each MG agent sends a reference value ($\omega_{\text{MGk}}/V_{fk}^*$) with pinning gain $g_{k1} = 1$ to DG$_{k1}$ in the communication network G_k of MG$_k$.
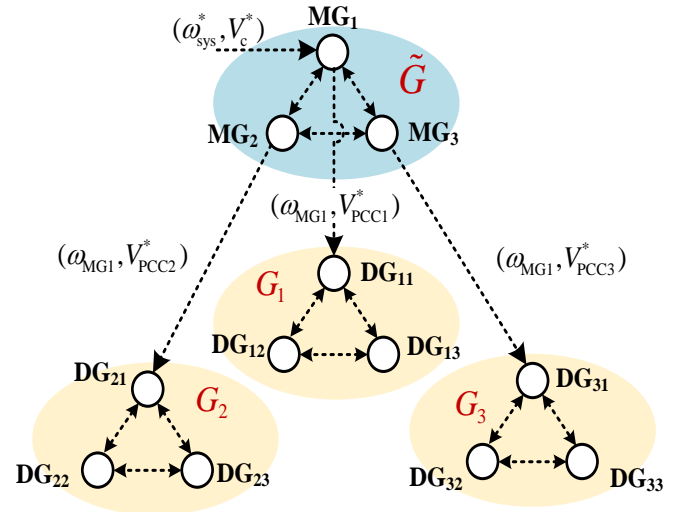

Fig. 5 Topology of two-layer distributed communication network

B. Eigen-Analysis Results

The system dynamics and stability analysis results with the

proposed control method are presented in this subsection.

1) Participation factors: Fig. 6 compares the low-frequency eigenvalue spectra of single MG_1, MG_2, MG_3 and the NMG system. Note that a single MG only employs the MG layer controllers in Section III, with ω_{MGk} and V^*_{PCCk} set as desired values. The typical dominant modes of the NMG system are labeled as mode i ($i = 1,2,...,8$).

Fig. 6 indicates that interconnecting MGs i) significantly change the shaping of the eigenvalues on the complex plane, ii) retain the single MG modes, i.e., MG modes 1-3, and iii) introduce four pairs of low-damping modes (modes 4-7), leading to many more oscillatory system responses compared with single MGs.
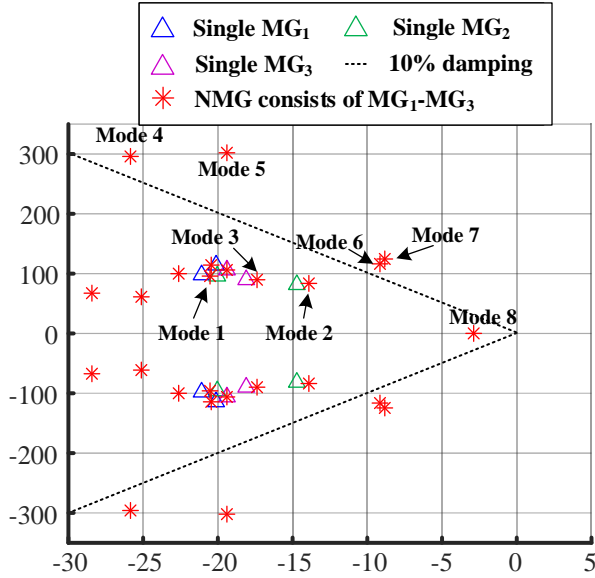

Fig. 6 Low-frequency eigenvalue spectra of three single MGs and NMG system

To identify the correlation between system states and dominant oscillatory modes, a participation factor analysis is conducted. The participation factor is calculated by multiplying corresponding elements in the right and left eigenvectors of the state matrix A_{sys}. This analysis can be used to measure the association between the state variables and the modes.

Fig. 7 illustrates the participation factors of MG layer states ($\Delta\delta_{ki}, \Delta P_{ki}, \Delta Q_{ki}, \Delta\Omega_{ki}, \Delta\lambda_{ki}, \Delta h_{ki}$), NMG layer states ($\Delta\delta_k, \Delta P_k, \Delta Q_k, \Delta\Omega_k, \Delta\lambda_k, \Delta h_k$) and the critical bus voltage controller state ($\Delta\psi$). As indicated by Fig. 7, mode 1 is a typical MG inner mode that is almost solely affected by states of DG_{11}~DG_{13} units within MG_1. Modes 5 and 7 are intercoupling modes mainly affected by states of both MG and NMG layers. For simplicity, the participation factors of modes 2 and 3 (MG inner modes of MG_2 and MG_3) and modes 4 and 6 (intercoupling modes) are not presented. In addition, mode 8 is mainly affected by the critical bus voltage controller. The strongly associated states, controllers and parameters with modes 1-8 are summarized in Table IV. Table IV indicates that the most dominant modes 4-7 (with damping less than 10%) are affected by the control parameters of DSCs and DQCs. Therefore, the impact of these parameters on system stability should be carefully analyzed.
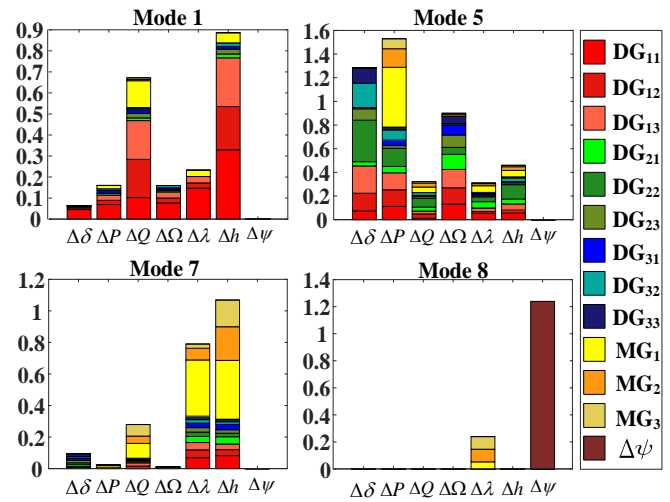

Fig. 7 Participation factors of modes 1, 5, 7 and 8

2) Sensitivity analysis of DSC and DQC parameters: Fig. 8 shows the traces of modes 4-7 as a function of c_{pki} and c_{qk}. The impacts of other DSC and DQC parameters are summarized in Table IV. Fig. 8 shows that the variation of parameters may bring instability risk to the system. The summary in Table IV indicates that a dominant mode may be affected by multiple controllers and their parameters. In addition, a control parameter may affect different modes.
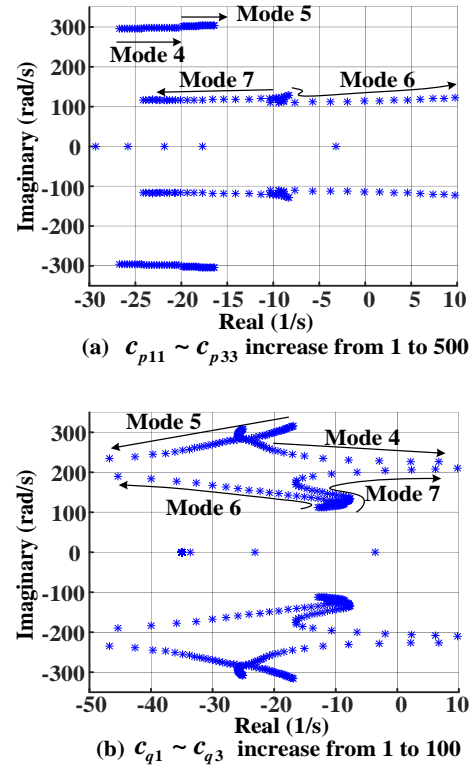

(a) $c_{p11} \sim c_{p33}$ increase from 1 to 500

(b) $c_{q1} \sim c_{q3}$ increase from 1 to 100

Fig. 8 Traces of the most dominant modes 4-7.

3) Summary: The above results reveal that i) interconnecting MGs introduces new low-frequency oscillatory modes and therefore complicates the system dynamic behavior; ii) the new low-damping modes (modes 4-7) reduce the stability margin due to the coupling among neighboring MGs and between the

TABLE IV. RESULTS OF PARTICIPATION FACTORS ANALYSIS

Modes	Strongly associated control layer	Strongly associated states	Associated controllers	Parameters of the associated controller	Impact of parameters on mode damping (MD)
1-3	MG layer-DSClevel	$\Delta Q_{ki}, \Delta \lambda_{ki}, \Delta h_{ki}$	(15),(25)	c_{vki}, c_{qki}	$c_{vki}, c_{qki} \uparrow$ (MD $\downarrow$)
4-5	MG layer-DSClevel	$\Delta Q_{ki}, \Delta \lambda_{ki}, \Delta h_{ki}$	(11),(15)	c_{vki}, c_{qki}	Mode 4: $c_{vki}, c_{qki}, c_{vk}, c_{qk} \uparrow$ (MD $\downarrow$);
	NMG layer-DQClevel	$\Delta Q_k, \Delta \lambda_k, \Delta h_k$	(22),(25)	c_{vk}, c_{qk}	Mode 5: $c_{vki}, c_{vk} \uparrow$ (MD $\downarrow$); $c_{qki}, c_{qk} \uparrow$ (MD $\uparrow$)
6-7	MG layer-DSClevel	$\Delta \delta_{ki}, \Delta P_{ki}, \Delta \Omega_{ki}$	(9)	$c_{\omega ki}, c_{pki}$	Mode 6: $c_{pki} \uparrow$ (MD $\downarrow$); $c_{\omega ki}, c_{qk} \uparrow$ (MD $\uparrow$)
	NMG layer-DQClevel	Δh_k	(25)	c_{qk}	Mode 7: $c_{qk} \uparrow$ (MD $\downarrow$); $c_{\omega ki}, c_{pki} \uparrow$ (MD $\uparrow$)
8	NMG layer-DQClevel	$\Delta \psi$	(23)	k_p, k_i	$k_p, k_i \uparrow$ (MD $\downarrow$); $k_p, k_i \downarrow$ (MD $\uparrow$)

two control layers; and iii) the dominant oscillatory modes are affected by multiple controllers. Note that the parameters in Table III are carefully tuned based on the guidelines in Table IV.

C. Time-Domain Simulation Results in PSCAD/EMTDC

Three cases are designed for the simulation. Case 1 demonstrates the steady-state performance of the proposed control strategy, namely, the capability to meet control objectives (i)-(iv) simultaneously under normal conditions. Case 2 verifies the system dynamic performance under communication failures as well as sudden load changes. Case 3 verifies the plug-and-plug functionality of DG and MG units.

1) Case 1 – steady-state performance: The PCs are initially engaged, the DSCs and TCs are activated at t=1.5 s, and DQCs are employed at t=3 s.
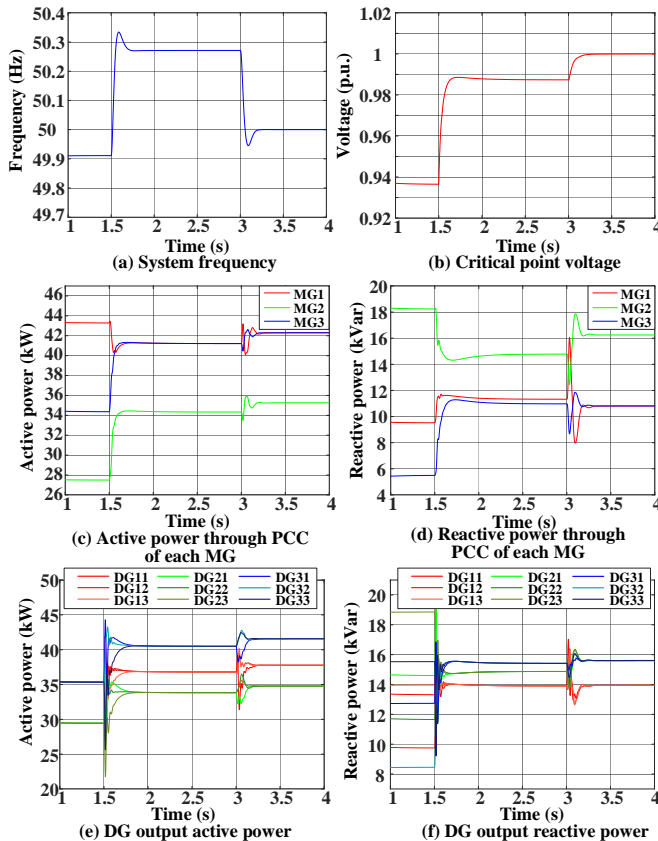

Fig. 9 Steady-state performance of the proposed method.

Fig. 9 (a) indicates that a 0.25 Hz frequency deviation is introduced by the TCs, while the DQCs restore the system frequency to 50 Hz (objective i). Fig. 9 (b) indicates that the critical bus voltage is restored to 1 p.u. by the DQC (objective ii). Fig. 9 (d) indicates that after t=3 s, the DQCs achieve accurate reactive power sharing among MGs with ratios of Q_1 to Q_3 being 2:3:2 (objective iii). Fig. 9 (f) indicates that after t=1.5 s, the DSCs realize accurate reactive power sharing among DGs within each MG, with ratios of Q_{k1} to Q_{k3} being 1:1:1 (objective iv). Fig. 9 (c) and (e) indicate that the output active powers of MGs and DGs are always accurately shared. Note that the power sharing ratios are presented in Table II.

2) Case 2 – communication link failures: In this case, all the controllers are activated at t=0.8 s, and then the system reaches a steady state. It is worth noting that, based on the proof in [34], for the tracking synchronization problem and regulator synchronization problem, if a spanning tree exists in the corresponding distributed communication network and $g_k \neq 0$ for at least one root node, the proposed controllers can reach a steady state, and objectives (i)~(iv) can still be realized.
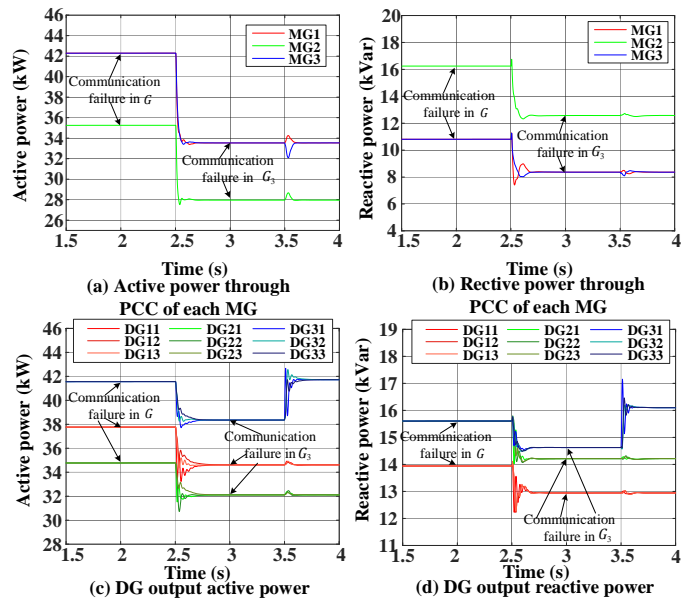

Fig. 10 System behaviors when communication failures occur in $\tilde{G}$ and G_3.

Stage 1 (1.5–3 s): in the upper communication network $\tilde{G}$, the communication link between MG₂ and MG₃, as shown in Fig. 5, fails at $t = 2$ s. Subsequently, 25% of load 9 is switched

off at t=2.5 s. The results in Fig. 10 show that the steady-state objectives (i)-(iv) can still be achieved after the communication link failure since the remaining communication network still contains a spanning tree.

Stage 2 (3–4 s): During this stage, a worse scenario, which refers to communication failures occurring in both upper network $\tilde{G}$ and lower network G_k, is set up. After one communication link fails at t=2 s in upper communication network $\tilde{G}$, for lower communication network G_3 in MG$_3$, the communication link between DG$_{32}$ and DG$_{33}$, as shown in Fig. 10, fails at t=3s Subsequently, at t=3.5 s, 80% of load 6, which is the internal load of MG$_3$, is switched on. The results in Fig. 10 show that the steady-state objectives (i)-(iv) can be realized since both the network $\tilde{G}$ and G_3 still contain a spanning tree after communication failure at this stage. In addition, Fig. 10 also indicates that the NMG system reaches a steady state within 0.5 s after a disturbance, and no significant overshoot is observed, even under communication failure events.

3) Case 3 – plug-and-plug operation: In this study, all the controllers are activated at t=0.8 s, and then the system reaches a steady state.
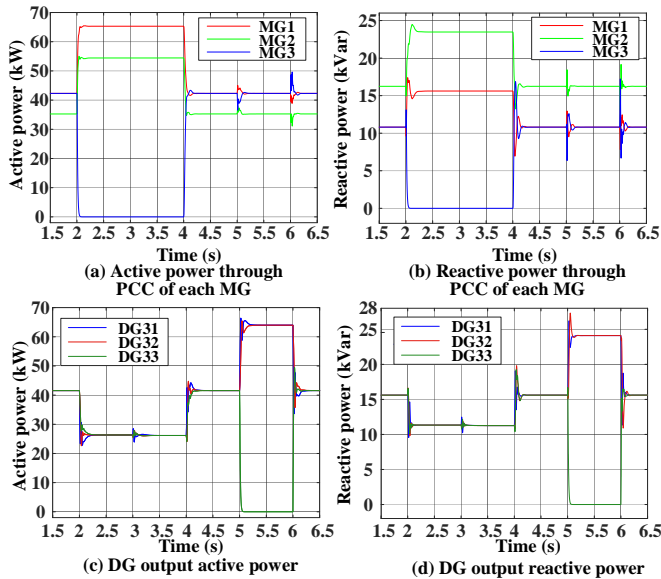

Fig. 11 System behaviors under plug-and-play operation of MG$_3$ and DG$_{33}$.

Stage 1 (2–4s): MG$_3$ is disconnected at t=2 s and reconnected at t=4 s to evaluate the plug-and-play capability of MGs. Note that (i) the MG will lose all the communication links with its neighboring units when it disconnects with the NMG system, then these links will recover after its reconnection; (ii) the synchronization process is necessary for MG$_3$ before its reconnection (specifically, in this study, the synchronization of MG$_3$ starts at t=3 s during its islanded state); (iii) the MGs will transfer to the islanded operation state with only MG layer controllers employed after the disconnection event at t=2 s, and the reference angular frequency $\omega_{\mathrm{MG}k}$ and reference PCC voltage $V_{\mathrm{PCC}k}^*$ will be set as the rated value $2*pi*50$ rad/s and 1.0 p.u, respectively, to maintain a stable operation of the islanded MG$_3$. The active and reactive power through PCC of each MG are presented in Fig. 11 (a) and (b), respectively.

Stage 2 (5–6 s): DG$_{33}$ in MG$_3$ disconnects at t=5 s and reconnects at t=6 s to evaluate the plug-and-play capability of the

DGs. Similarly, DG$_{33}$ will lose all the communication links with its neighboring units when it disconnects, and the communication links will recover after its reconnection. The synchronization process of DG$_{33}$ starts immediately after it disconnects at t=5 s. The active and reactive power of DG units in MG$_3$ are presented in Fig. 11 (c) and (d), respectively.

The above results show that after the disconnection of MG$_3$ in the NMG layer and DG$_{33}$ in the MG layer, objectives (i)~(iv) can still be realized (for the sake of simplicity, only the results of active and reactive power are given). This is because the remaining communication network $\tilde{G}$ of the NMG-control layer and G_3 of the MG-control layer still contain a spanning tree. After MG$_3$ and DG$_{33}$ reconnect, their power sharing objectives can be realized. In addition, during plug-and-play operation, no significant overshoots are observed, and the time of recovering to a steady state is within 0.4 s.

VI. EXPERIMENTAL VALIDATION

This section provides experimental results to validate the practical implementation feasibility of the proposed methods.

A. Experimental setup

Fig. 12 shows the experimental NMG system setup, which includes a real-time dSPACE 1006 platform, four Danfoss inverters, resistive loads, inductive loads, line impedances, switches and a control desk. The control strategy is programmed and executed in the dSPACE 1006 platform to switch the inverters. The switching frequency is 10 kHz.
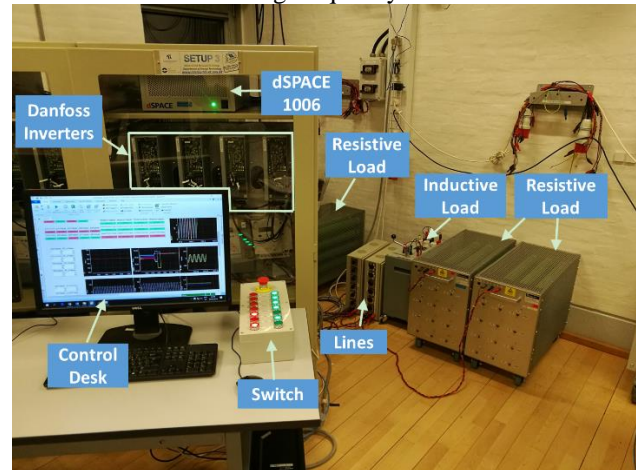

Fig. 12 Experimental setup in the laboratory

The physical configuration of the experimental NMG system is shown in Fig. 13. There are two microgrids in the system, and each microgrid consists of two DG units. The circuit breakers CB$_1$ and CB$_2$ are closed. MG$_1$ and MG$_2$ are connected to the critical bus through line impedances. The system rated frequency is 50 Hz, and the rated rms voltage is 200 V.

Table V provides the electrical parameters of the experimental NMG system. The parameters of the four level controllers are shown in Tables VI and VII. From Table VI, it can be seen that (i) the active and reactive power capacities between MG$_1$ and MG$_2$ are equal, i.e., $P_{\mathrm{sMG1}} = P_{\mathrm{sMG2}}$ and $Q_{\mathrm{sMG1}} = Q_{\mathrm{sMG2}}$, and (ii) the ratios of the active and reactive power capacities between DG$_{k1}$ and DG$_{k2}$ are both 4:3, i.e., $P_{\mathrm{max}k1}:P_{\mathrm{max}k2} = 4:3$ and $Q_{\mathrm{max}k1}:Q_{\mathrm{max}k2} = 4:3$, $k = 1, 2$.

Fig. 14 shows the topology of two-layer distributed communication networks for the experimental NMG system. In the upper network $\tilde{G}$, MG$_1$ receives reference values ω_{sys}^* and V_c^*. In the lower network G_1 and G_2, DG$_{11}$ and DG$_{21}$ receive the references from $\tilde{G}$.
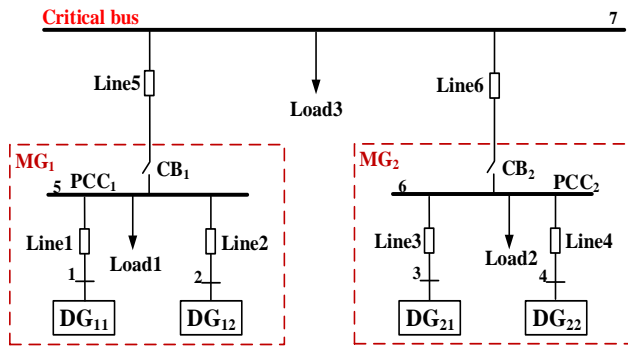

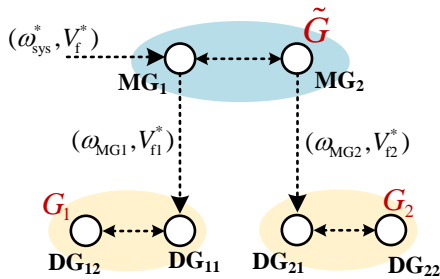Fig. 13 Physical configuration of the experimental NMG system

Fig. 14 Topology of the two-layer distributed communication network for the experimental NMG system

TABLE V. ELECTRICAL PARAMETERS OF EXPERIMENTAL NMG SYSTEM

Inverter	Filter inductance: 1.8 mH Filter capacitance: 27 μF
Line	Line 1 = 1.8 mH, Line 2 = 1.8 mH, Line 3 = 1.8 mH, Line 4 = 1.8 mH, Line 5 = 1.9 Ω + 2.5 mH, Line 6 = 1.6 Ω + 2.1 mH
Load	Load 1 = 92 Ω, Load 2 = 153.3 Ω, Load 3 = 38.1 + j32.9 Ω

TABLE VI. PARAMETERS OF PCs AND TCs FOR THE EXPERIMENTAL SYSTEM

Parameters	DG$_{11}$	DG$_{12}$	DG$_{21}$	DG$_{22}$	MG$_1$	MG$_2$
D_{Pki}/D_{Pk} (Hz/W·10^{-3})	0.625	0.833	0.625	0.833	0.357	0.357
D_{Qki}/D_{Qk} (V/Var·10^{-3})	6.479	8.639	6.479	8.639	3.702	3.702
P_{max}/P_{sMG} (kW)	1.8	1.35	1.8	1.35	3.15	3.15
Q_{max}/Q_{sMG} (kvar)	1.2	0.9	1.2	0.9	2.1	2.1

TABLE IV. PARAMETERS OF DSCs AND DQCs FOR EXPERIMENTAL SYSTEM

| Parameters	DSC level	DQC level
$c_{\omega ki}/c_{\omega k}$	400	80
c_{pki}/c_{pk}	400	80
c_{vki}/c_{vk}	150	30
c_{qki}/c_{qk}	20	2
k_{pk}/k_p	1.2	0.3
k_{ik}/k_i	42	10

B. Experimental results

The system is initially operated with PC. At t=6.9 s, the DSC and TC are activated, and at t=8.55 s, the DQC is activated. Fig. 15 shows the corresponding experimental results. Fig. 15(a) and (b) indicate that after t=8.55 s, the DQC can restore the system frequency and critical bus voltage to their rated values of 50 Hz and 1 p.u., i.e., objectives (i) and (ii) are realized. Fig. 15(c) indicates that the active powers through the PCC of each MG are equal after applying TC at t=6.9 s (objective (iii)-(1)). Fig. 15(d) indicates that the reactive powers through PCC of each MG are equal after applying DQC at t=8.55 s (objective (iii)-(2)). Fig. 15(e) and (f) indicate that after applying DSC at t=6.9 s, the output active power and reactive power of DG units in each MG can realize accurate sharing with $P_{k1}:P_{k2}$ and $Q_{k1}:Q_{k2}$ both being 4:3 (objective (iv)).
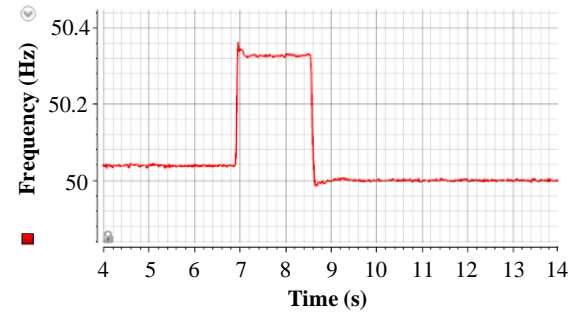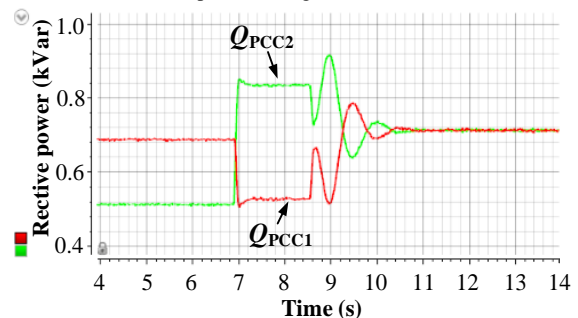

(a) system frequency
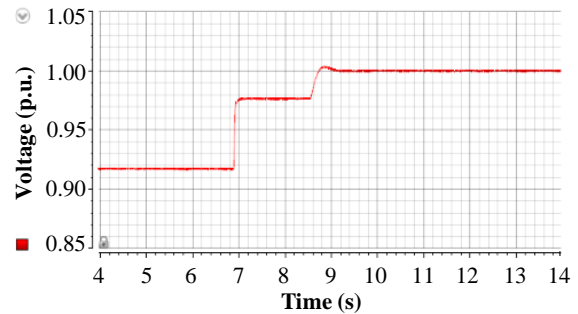
(b) Critical bus voltage
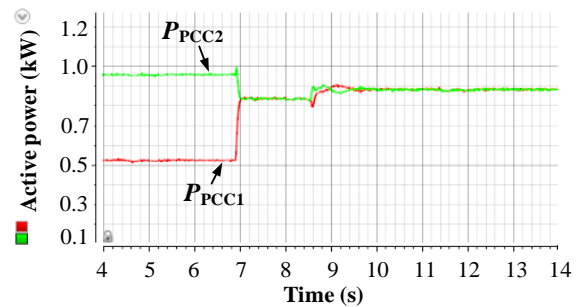
(c) Active power through PCC of each MG

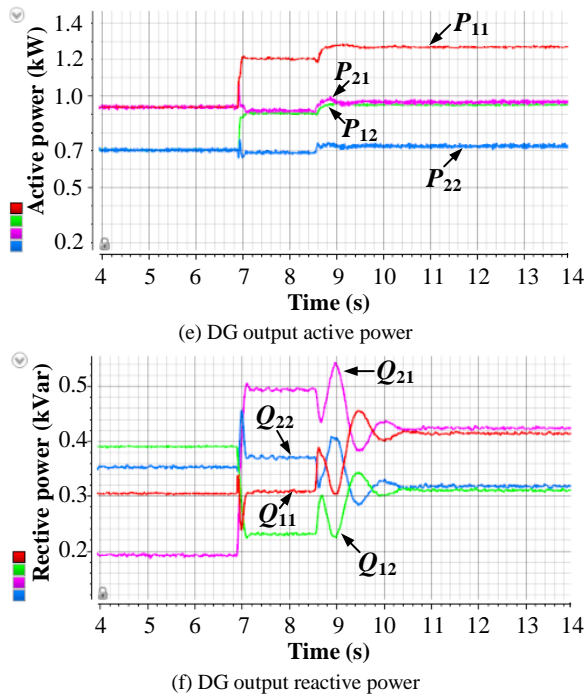(d) Reactive power through PCC of each MG

(e) DG output active power

(f) DG output reactive power

Fig. 15 Experimental results (DSC and TC are activated at t=6.9 s, and DQC is activated at t=8.55 s)

VII. Conclusion

This paper presents a hierarchical and distributed cooperative control architecture and method for islanded NMG systems. The proposed two-layer and four-level control architecture is capable of protecting the proprietary information and enabling the plug-and-play capability of each MG. Based on this architecture, the proposed two-layer distributed cooperative control method can simultaneously meet multiple objectives, including the regulation of frequency and critical bus voltage, as well as accurate power sharing in both the MG and NMG layers. In addition, this paper also develops a detailed small-signal dynamic model of the NMG system considering the distributed control method and multiple control layers. The corresponding small-signal stability analysis reveals that i) interconnecting MGs results in low-damping and intercoupling modes, which may lead to system instability, and ii) the system dominant modes are strongly affected by controller parameters, especially those in the DSC and DQC levels. Finally, time-domain simulation as well as experimental results on an NMG test system validate the effectiveness of the proposed methods.

Appendix

The communication networks of the NMG system can be modeled by several directed graphs (digraphs), where the DG units (or MG units) are considered as the nodes of the communication digraphs.

The lower communication networks are deployed with the MG layer, which contains m digraphs, G_1, $G_2 \dots G_m$, corresponding to m MGs. The digraph for the kth MG is expressed as $G_k = (\mathcal{V}^k, \mathcal{E}^k, \mathcal{A}^k)$, with a non-empty finite set of n_k DG nodes $\mathcal{V}^k = \{\mathcal{V}_1^k, \mathcal{V}_2^k, \dots, \mathcal{V}_{S_k}^k\}$, a set of edges $\mathcal{E}^k \in \mathcal{V}^k \times \mathcal{V}^k$,

and the associated adjacency matrix $\mathcal{A}^k = [a_{ij}]$. Note that the DG units are considered nodes of the communication digraph. An edge from node j to node i is denoted by $(\mathcal{V}_j^k, \mathcal{V}_i^k)$, which indicates that node i receives information from node j. a_{ij} is the weight of edge $(\mathcal{V}_j^k, \mathcal{V}_i^k)$, and $a_{ij} > 0$ if $(\mathcal{V}_j^k, \mathcal{V}_i^k) \in \mathcal{E}^k$; otherwise, $a_{ij} = 0$. Node j is a neighbor of node i if $(\mathcal{V}_j^k, \mathcal{V}_i^k) \in \mathcal{E}^k$. The set of neighbors of node i is denoted as $\mathcal{L}_i^k = \{j \mid (\mathcal{V}_j^k, \mathcal{V}_i^k) \in \mathcal{E}^k\}$.

The upper communication network is deployed with the NMG layer, which has only one digraph $\tilde{G}$. Each MG unit is considered a node of this digraph. Similarly, this digraph is expressed as $\tilde{G} = (\tilde{\mathcal{V}}, \tilde{\mathcal{E}}, \tilde{\mathcal{A}})$ with nodes set $\tilde{\mathcal{V}} = \{\tilde{\mathcal{V}}_1, \tilde{\mathcal{V}}_2, \dots, \tilde{\mathcal{V}}_M\}$, edges $\tilde{\mathcal{E}} \in \tilde{\mathcal{V}} \times \tilde{\mathcal{V}}$, and the associated adjacency matrix is $\tilde{\mathcal{A}} = [\tilde{a}_{kl}]$. Node l is a neighbor of node k if $(\tilde{\mathcal{V}}_l, \tilde{\mathcal{V}}_k) \in \tilde{\mathcal{E}}$. The set of neighbors of node k is denoted as $\mathcal{H}_k = \{l \mid (\tilde{\mathcal{V}}_l, \tilde{\mathcal{V}}_k) \in \tilde{\mathcal{E}}\}$.

A directed path from node $i(k)$ to node $j(l)$ is a sequence of edges. A digraph has a spanning tree if there is a node i_r (called the root node), such that there is a directed path from the root node to every other node in the graph.

References

[1] U.S. Department of Energy and National Energy Technology Laboratory, Operates Resiliently Against Attack and Natural Disaster [Online]. Available: http://www.smartgridinformation.info/pdf/1438_doc_1.pdf.

[2] Y. Xu, C. C. Liu, K. Schneider, F. Tuffner, and D. Ton, "Microgrids for Service Restoration to Critical Load in a Resilient Distribution System," *IEEE Trans. Smart Grid*, vol. 9, no. 1, pp. 426-437, Jan. 2018.

[3] C. Yuen, A. Oudalov and A. Timbus, "The Provision of Frequency Control Reserves from Multiple Microgrids," *IEEE Trans. Ind. Electron.*, vol. 58, no. 1, pp. 173-183, Jan. 2011.

[4] K. P. Schneider, F. K. Tuffner, M. A. Elizondo, C. C. Liu, Y. Xu , S. Backhaus, and D. Ton, "Enabling Resiliency Operations Across Multiple Microgrids With Grid Friendly Appliance Controllers," *IEEE Trans. Smart Grid*, vol. 9, no. 5, pp. 4755-4764, Sep. 2018.

[5] J. Lopes, A. Madureira, N. Gil, and F. Resende. "Chapter 5: Operation of Multi-Microgrids" in *Microgrids Architecture and Control*, Chichester, UK: John Wiley and Sons Ltd, 2014.

[6] X. Wu, X. Wu, Y. Xu, and J. He, "A Hierarchical Control Architecture for Islanded Multi-Microgrid Systems," *2018 IEEE Power and Energy Society General Meeting (PESGM)*, Portland, OR, 2018.

[7] J. M. Guerrero, J. C. Vasquez, J. Matas, L. G. de Vicuna, and M. Castilla, "Hierarchical Control of Droop-controlled AC and DC Microgrids—a General Approach toward Standardization," *IEEE Trans. Ind. Electron.*, vol. 58, no. 1, pp. 158-172, Jan. 2011.

[8] D. E. Olivares *et al*., "Trends in Microgrid Control," *IEEE Trans. Smart Grid*, vol. 5, no. 4, pp. 1905-1919, Jul. 2014.

[9] Pogaku, M. Prodanovic, and T. C. Green, "Modeling, Analysis and Testing of Autonomous Operation of an Inverter-Based Microgrid," *IEEE Trans. Power Electron.*, vol. 22, no. 2, pp. 613-625, Mar. 2007.

[10] Y. W. Li and C. N. Kao, "An Accurate Power Control Strategy for Power-Electronics-Interfaced Distributed Generation Units Operating in a Low-Voltage Multibus Microgrid," *IEEE Trans. Power Electron.*, vol. 24, no. 12, pp. 2977-2988, Dec. 2009.

[11] J. M. Guerrero, L. G. Vicuna, J. Matas, M. Castilla, and J. Miret, "Output Impedance Design of Parallel-connected UPS Inverters with Wireless Load-sharing Control," *IEEE Trans. Ind. Electron.*, vol. 52, no. 4, pp. 1126-1135, Aug. 2005.

[12] F. Katiraei, M. R. Iravani, and P. W. Lehn, "Micro-grid Autonomous Operation during and Subsequent to Islanding Process," *IEEE Trans. Power Delivery*, vol. 20, no. 1, pp. 248-257, Jan. 2005.

[13] G. Magdy, Emad A. Mohamed, G. Shabib, Adel A. Elbaset, Yasunori Mitani, "Microgrid dynamic security considering high penetration of renewable energy," *Protection and Control of Modern Power Syst.*, vol. 3, no. 1, pp. 1-11, Dec. 2018.

[14] Baoze Wei, J. C. Vásquez, J. M. Guerrero and Xiaoqiang Guo, "Control architecture for paralleled current-source-inverter (CSI) based uninterruptible power systems (UPS)," *in 2016 IEEE 8th Int. Power Electron. and Motion Control Conf.*, Hefei, 2016, pp. 151-156.

[15] M. S. Golsorkhi, D. J. Hill, and H. R. Karshenas, "Distributed Voltage Control and Power Management of Networked Microgrids," *IEEE J. Emerg. Sel. Topics Power Electron.*, to be published.

[16] W. Liu, W. Gu, Y. Xu, Y. Wang, and K. Zhang, "General Distributed Secondary Control for Multi-microgrids with both PQ-controlled and Droop-controlled Distributed Generators," *IET Generation, Transmission & Distribution*, vol. 11, no. 3, pp. 707-718, Feb. 2017.

[17] D. O. Amoateng, M. Al Hosani, M. S. Elmoursi, K. Turitsyn, and J. L. Kirtley, "Adaptive Voltage and Frequency Control of Islanded Multi-Microgrids," *IEEE Trans. Power Syst.,* vol. 33, no. 4, pp. 4454-4465, Dec. 2018.

[18] E. Pashajavid, F. Shahnia and A. Ghosh, "Development of a Self-Healing Strategy to Enhance the Overloading Resilience of Islanded Microgrids," *IEEE Trans. Smart Grid*, vol. 8, no. 2, pp. 868-880, Mar. 2017.

[19] F. Zhang, "Operation Of Networked Microgrids in the Electrical Distribution System," M.S. thesis, Dept. Elect. Eng. Comput. Sci, Case Western Reserve Univ., Cleveland, OH, 2016.

[20] N. J. Gil and J. A. P. Lopes, "Hierarchical Frequency Control Scheme for Islanded Multi-Microgrids Operation," *in 2007 IEEE Lausanne Power Tech*, Lausanne, Switzerland, 2007, pp. 473-478.

[21] R. Zamora, "Energy Management and Multi-layer Control for Networked Microgrids," Ph.D. dissertation, Dept. Elect. Eng. Comput. Sci, Washington State Univ., WA, 2015.

[22] R. Zamora and A. K. Srivastava, "Multi-Layer Architecture for Voltage and Frequency Control in Networked Microgrids," *IEEE T. Smart Grid,* vol. 8, no. 2, pp. 2076 - 2085, May. 2018.

[23] R. Majumder and G. Bag, "Parallel operation of converter interfaced multiple microgrids," *Int. J. Elect. Power & Energy Sys.*, vol. 55, pp. 486-496, Aug. 2014.

[24] I. U. Nutkani, F. Blaabjerg and P. C. Loh, "Power flow control of intertied ac microgrids," *IET Power Electron.,* vol. 6, no. 7, pp. 1329-1338, Aug. 2013.

[25] Y. Zhang and L. Xie, "Online Dynamic Security Assessment of Microgrid Interconnections in Smart Distribution Systems," *IEEE Trans. Power Syst.,* vol. 30, no. 6, pp. 3246-3254, Nov. 2015.

[26] Y. Zhang, L. Xie, and Q. Ding, "Interactive Control of Coupled Microgrids for Guaranteed System-Wide Small Signal Stability," *IEEE Trans. Smart Grid*, vol. 7, no. 2, pp. 1088-1096, Mar. 2016.

[27] M. J. Hossain, M. A. Mahmud, F. Milano, S. Bacha, and A. Hably, "Design of Robust Distributed Control for Interconnected Microgrids," *IEEE Trans. Smart Grid,* vol. 7, no. 6, pp. 2724-2735, Nov. 2016.

[28] I. U. Nutkani, P. C. Loh and F. Blaabjerg, "Distributed Operation of Interlinked AC Microgrids with Dynamic Active and Reactive Power Tuning," *IEEE T. Ind. Appl.,* vol. 49, no. 5, pp. 2188-2196, Sep. 2013.

[29] X. Lu, J. Lai, X. Yu, Y. Wang, and J. M. Guerrero, "Distributed Coordination of Islanded Microgrid Clusters Using a Two-layer Intermittent Communication Network," *IEEE Trans. Ind. Informat.*, vol. 14, no. 9, pp. 3956-3969, Sep. 2018.

[30] F. O. Resende, N. J. Gil and J. A. P. Lopes, "Service restoration on distribution systems using Multi-MicroGrids," *Eur. Trans. Elect. Power*, vol. 21, no. 2, pp. 1327-1342, Mar. 2011.

[29] G. Liu, M. R. Starke, B. Ollis, and Y. Xue. (2016, Oct.). "Networked Microgrids Scoping Study," ORNL, TN.[Online]. Available: https://info.ornl.gov/ sites/publications/files/Pub68339.pdf.

[30] Z. Haibo, Z. Boming, S. Hongbin and A. Ran, "A new distributed power flow algorithm between multi-control-centers based on asynchronous iteration," *2006 International Conference on Power System Technology, Chongqing*, 2006, pp. 1-7.

[31] R. Olfati-Saber, J. A. Fax, and R. M. Murray, "Consensus and Cooperation in Networked Multi-Agent Systems," *Proc. IEEE*, vol. 95, no. 1, pp. 215-233, Jan. 2007.

[32] Z. Zhao, P. Yang, Y. Wang, Z. Xu, and J. M. Guerrero, "Dynamic Characteristics Analysis and Stabilization of PV-Based Multiple Microgrid Clusters," *IEEE Trans. Smart Grid*, vol. 10, no. 1, pp. 805-818, Jan. 2019.

[33] Z. Li, Z. Duan, G. Chen, and L. Huang, "Consensus of Multiagent Systems and Synchronization of Complex Networks: A Unified Viewpoint," *IEEE Trans. Circuits Syst. I, Reg. Papers*, vol. 57, no. 1, pp. 213-224, Jan. 2010.

[34] A. Bidram, A. Davoudi, F. L. Lewis and Z. Qu, "Secondary control of microgrids based on distributed cooperative control of multi-agent systems," *IET Generation, Transmission & Distribution,* vol. 7, no. 8, pp. 822-831, Aug. 2013.

VIII. BIOGRAPHIES
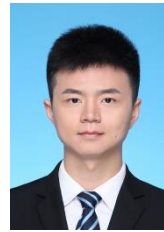
Xiaoyu Wu (S'15) received his B.S degree in electrical engineering from Beijing Jiaotong University, Beijing, China, in 2013.

He is currently pursuing his Ph.D. degree at Beijing Jiaotong University, Beijing, China. During 2015-2016, he was a visiting scholar at the North Carolina State University, Raleigh, NC, USA. His research interests include demand response, control and stability analysis of microgrid.

Yin Xu (S'12–M'14-SM'18) received his B.E. and Ph.D. degrees in electrical engineering from Tsinghua University, Beijing, China, in 2008 and 2013, respectively.

He is currently a Professor with the School of Electrical Engineering at Beijing Jiaotong University, Beijing, China. During 2013–2016, he was an Assistant Research Professor with the School of Electrical Engineering and Computer Science at Washington State University, Pullman, WA, USA. His research interests include power system resilience, distribution system restoration, power system electromagnetic transient simulation, and AC-DC hybrid power systems.

Dr. Xu is currently serving as Secretary of the Distribution Test Feeder Working Group under the IEEE PES Distribution System Analysis Subcommittee.

Xiangyu Wu (S'13-M'17) received the B.S. degree from the Department of Electrical Engineering, Zhejiang University, Hangzhou, China, in 2012 and the Ph.D. degree in electrical engineering from Tsinghua University, Beijing, China, in 2017.

He is currently a postdoctoral researcher at the School of Electrical Engineering, Beijing Jiaotong University, Beijing, China. In 2015, he was a visiting scholar at University of Toronto, Toronto, ON, Canada. Since 2018, he is a guest researcher at the Department of Energy Technology, Aalborg University, Aalborg, Denmark. His research interests include the control and stability analysis of microgrid and power electronic based power systems.

Jinghan He (M'07-SM'18) received the M.Sc. degree in electrical engineering from the Tianjin University, Tianjin, China, in 1994 and the Ph.D. degree in electrical engineering from Beijing Jiaotong University, Beijing, China, in 2007.

She is currently a Professor at Beijing Jiaotong University, Beijing, China. Her main research interests are protective relaying, fault distance measurement, and location in power systems.

Josep M. Guerrero (S'01-M'04-SM'08-FM'15) received the B.S. degree in telecommunications engineering, the M.S. degree in electronics engineering, and the Ph.D. degree in power electronics from the Technical University of Catalonia, Barcelona, in 1997, 2000 and 2003, respectively. Since 2011, he has been a Full Professor with the Department of Energy Technology, Aalborg University, Denmark, where he is responsible for the Microgrid Research Program (www.microgrids.et.aau.dk). From 2014 he is chair Professor in Shandong University; from 2015 he is a distinguished guest Professor in Hunan University; and from 2016 he is a visiting professor fellow at Aston University, UK, and a guest Professor at the Nanjing University of Posts and Telecommunications.

His research interests is oriented to different microgrid aspects, including power electronics, distributed energy-storage systems, hierarchical and cooperative control, energy management systems, smart metering and the internet of things for AC/DC microgrid clusters and islanded minigrids; recently specially focused on maritime microgrids for electrical ships, vessels, ferries and seaports. Prof. Guerrero is an Associate Editor for a number of IEEE TRANSACTIONS. He has published more than 450 journal papers in the fields of microgrids and renewable energy systems, which are cited more than 30,000 times. He received the best paper award of the IEEE Transactions on Energy Conversion for the period 2014-2015, and the best paper prize of IEEE-PES in 2015. As well, he received the best paper award of the Journal of Power Electronics in 2016. During five consecutive years, from 2014 to 2018, he was awarded by Thomson Reuters as Highly Cited Researcher. In 2015 he was elevated as IEEE Fellow for his contributions on "distributed power systems and microgrids."

Chen-Ching Liu (S'80–M'83–SM'90–F'94) received the Ph.D. degree from the University of California, Berkeley, CA, USA, in 1983.

He served as a Professor with the University of Washington, Seattle, WA, USA, from 1983–2005. During 2006–2008, he was Palmer Chair Professor with Iowa State University, Ames, IA, USA. During 2008–2011, he was a Professor and Acting/Deputy Principal of the College of Engineering, Mathematical and Physical Sciences with University College Dublin, Ireland. He was Boeing Distinguished Professor of Electrical Engineering and Director of the Energy Systems Innovation Center, Washington State University, Pullman, WA, USA. Currently, he is American Electric Power Professor and Director of the Center for Power and Energy, Virginia Polytechnic Institute and State University, Blacksburg, VA, USA. He is also a Research Professor at Washington State University.

Prof. Liu was the recipient of the IEEE PES Outstanding Power Engineering Educator Award in 2004. In 2013, he received the Doctor Honoris Causa from Polytechnic University of Bucharest, Romania. He served as Chair of the IEEE PES Technical Committee on Power System Analysis, Computing, and Economics during 2005–2006. He is a Fellow of the IEEE.

Kevin P. Schneider (S'00–M'06–SM'08) received his B.S. degree in Physics and M.S. and Ph.D. degrees in Electrical Engineering from the University of Washington, Seattle, WA, USA.

He is currently a Principal Research Engineer with the Pacific Northwest National Laboratory, working at the Battelle Seattle Research Center, Seattle, WA, USA. He is an Adjunct Faculty member with Washington State University, Pullman, WA, USA, and an Affiliate Assistant Professor with the University of Washington, Seattle, WA, USA. His main areas of research are distribution system analysis and power system operations.

Dr. Schneider is a licensed Professional Engineer in Washington State. He is the past Chair of the Distribution System Analysis Sub-Committee and current Secretary of the Power System Analysis, Computing, and Economics (PSACE) Committee.

Dan T. Ton received his B.S. degree is in electrical engineering and M.S. degree in business management from the University of Maryland, Baltimore, MD, USA.

He is a Program Manager of Smart Grid R&D within the U.S. Department of Energy (DOE) Office of Electricity Delivery and Energy Reliability (OE). He is responsible for developing and implementing a multi-year R&D program plan for next-generation smart grid technologies to transform the electric grid in the United States through public/private partnerships. Previously, he managed the Renewable Systems Integration program within the DOE Solar Energy Technologies Program.